Eur. Phys. J. Appl. Phys. **84**, 10903 (2018)

https://doi.org/10.1051/epjap/2018180271

THE EUROPEAN PHYSICAL JOURNAL APPLIED PHYSICS

Regular Article

Experimental investigation of drag coefficient of free-falling deformable liquid gallium droplet★

M. Sofwan Mohamad[1,2], C.M. Mackenzie Dover[1], and K. Sefiane[1,*]

[1] Institute for Multiscale Thermofluids, School of Engineering, University of Edinburgh, Faraday Building, King's Buildings, EH9 3DW, UK

[2] School of Mechatronic Engineering, Universiti Malaysia Perlis (UniMAP), Kampus Pauh Putra, 02600 Arau, Perlis, Malaysia

Received: 19 September 2018 / Received in final form: 30 October 2018 / Accepted: 31 October 2018

Abstract. In this article, the effect of shape and deformation on the drag coefficient of a free-falling liquid gallium droplet in water in a terminal state is investigated experimentally. The temperature of the dispersed and continuous liquid was varied in order to examine the effect on the liquid–metal droplets. The falling droplets were imaged using a high-speed camera, and a simple model was developed to predict drag coefficient over a Reynolds number range of $10^3 < Re < 10^4$. The drag coefficients of the deformed liquid gallium droplets were found to be larger than that associated with a solid sphere and the associated Weber number was below 4.5. It was found that the shape of all droplets in our experiment were oblate spheroid. A correlation has been established to predict the aspect ratio of a liquid gallium droplet moving in quiescent water. The deformation is highly dependent on interfacial surface tension and inertial force, while the viscosity ratio and pressure distribution have negligible effect.

1 Introduction

The motion and deformation of liquid droplets is important to numerous industrial applications and as a result has attracted considerable research interest. In industrial engineering, understanding the dynamics of liquid droplets is relevant to many applications such as the liquid sprays injected into combustion engines [1], ink-jet printers [2], microfluidics [3] and cooling systems [4]. Among various droplet materials, gallium and its alloys have drawn huge attention recently because of the associated physical and chemical properties such as low-melting points (liquid state at or near room temperature) and high thermal conductivities. Such characteristics offer tremendous opportunities for developing advanced technologies in newly emerging areas such as electronic cooling [4,5], 3D printing and printed electronics [6], flexible devices [7], soft actuators for robotics [8] and adhesion [9].

Hydrodynamic drag is of major importance to countless industrial practices as it is one of the most significant parameters that govern the movement of a droplet through a liquid and reducing it could lead to a substantial energy saving. To date, a substantial amount of literature can be found on this topic. However, reported data on the dynamics of deformable droplet are limited. References [10–12] present an extensive review of theory, experimental data and relevant approximations representing the characteristics of single droplet in fluid systems. As yet, there has been no systematic investigation on the effect of liquid gallium droplet morphology on the velocity and drag coefficient to the knowledge of the authors. In the following, the dynamics of a free-falling droplet of gallium in water are studied and the effect of droplet morphology on the velocity and drag coefficient are quantified. Characterising the relationship between the dynamics of the gallium droplets and the medium it is moving through facilitates a superior control of forces that inhibit droplet motion and the correlation can be applied to a number of systems.

2 Experimental setup

An experimental setup was designed to measure the terminal velocity of the falling droplets, a schematic of which is shown in Figure 1. The setup comprises a square cross-section, straight-walled column with closed bottom filled with water. The column is 1000 mm in height and 70.45 mm in inner side width. These dimensions were selected such that a droplet having diameter of less than 7 mm can fall through the continuous liquid with minimal wall effects, terminal velocity could be reached and end effects could be avoided [13,14]. The column is made of clear Perspex, allowing the motion of the falling droplets to be recorded by a high-speed camera. The bottom part of the column is inclined towards a central discharge point where a liquid gallium retrieval mechanism is located. The liquid gallium retrieval mechanism consists of two ball valves. This allowed for the liquid gallium to be removed

★ Contribution to the topical issue "Materials for Energy harvesting, conversion and storage (Icome 2017)", edited by Jean-Michel Nunzi, Rachid Bennacer, and Mohammed El Ganaoui.

* e-mail: ksefiane@ed.ac.uk

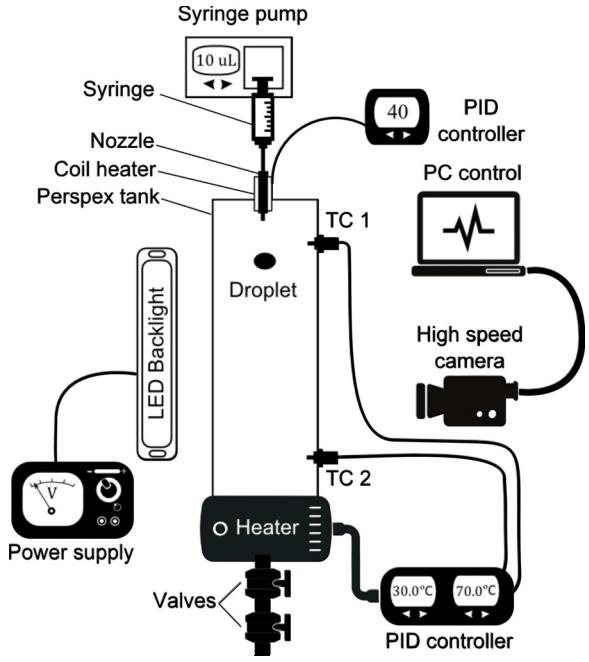

Fig. 1. Experimental setup.

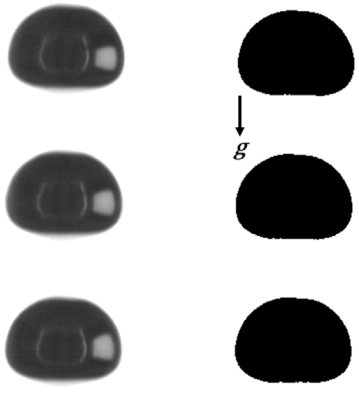

(a) Original image (b) Treated image

Fig. 2. Shape of liquid gallium droplets at terminal condition.

with a minimal amount of water being discharged from the column. An electric heater is fitted at the bottom part of the column and the water temperature inside the tank is controlled by a proportional-integral-derivative (PID) controller connected to two thermocouple probes that are situated at the top and bottom of the chamber. The water in the tank can be heated up to about 80 °C. In order to minimise the effect of thermal convection during experiments, the heater was turned off after heating the water to the required temperature. A few minutes later the temperature of water was found to be homogeneous at ±1 °C.

Liquid gallium was heated to the desired temperature and then fed from a syringe into the column of water. A precise volume of liquid gallium was released gradually, directly below the water surface to create a droplet with the help of a programmable syringe pump (Cole-Parmer Touch-Screen Syringe Pump 78-8110C). The accuracy of the syringe pump is ±0.355% with reproducibility of ±0.05%. Droplets were increased in volume until they detached from the needle due to their weight, and needles of different diameters could be attached to change the size of the examined droplet. The droplet behaviour during free fall was recorded by a high-speed CMOS camera (Nanosense MKIII) with frequency up to 1024 fps at a resolution of 1280 × 1024 pixels. The camera was coupled with an Edmund optics double gauss lens (54-691) to produce low distortion images. A custom-made 100 W LED light (Maxilux ProStrip120-High Power) was placed at about 40 mm behind the column to illuminate the test region.

The image sequences were converted into 8-bit grey scale, background-subtracted and thresholded such that spheres appeared as a black dot on a white background to allow for tracking and quantification of droplets using an in-house ImageJ macro. Information such as the relative position, velocity and diameter were obtained using automated analysis of this type. Figure 2 shows a series of images pre- and post-processing.

Table 1. Equivalent diameter of liquid gallium droplets used in experiment.

Volume (μl)	Equivalent diameter (mm)
17	3.19
60	4.86
90	5.56

3 Results and discussion

3.1 Diameter of the droplet

The diameter of the droplet can be calculated from a known dispersed volume of gallium. Volume equivalent diameter, $d_{\mathrm{eq}} = \sqrt[3]{\frac{3V}{4\pi}}$, can be calculated with the assumption that the droplet is a solid sphere symmetric about the major and minor axes plane of observation. Table 1 summarises the calculated diameter of liquid gallium droplets of various volumes. The calculated equivalent diameters are a convenient parameter to represent the droplets as well as to understand the effect of deformation on drag coefficient.

3.2 Droplet terminal velocity

Figure 3 shows co-plots of the velocity of free-falling liquid gallium droplets of various diameters in water as a function of their distance from the needle. It can be seen that the velocity becomes terminal after 200 mm for all sizes of droplets examined. After analysing the droplet's velocity under different thermal conditions, it was observed that each droplet in the investigation could attain a terminal condition after falling a distance of 200 mm. Hence, the

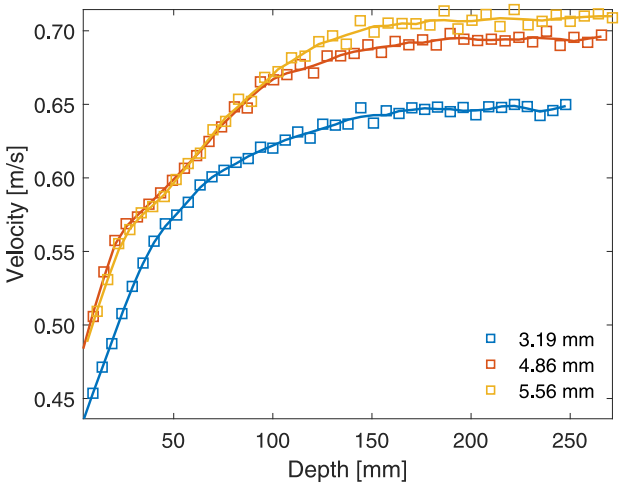

Fig. 3. Liquid gallium droplet's velocity as a function of their distance from the needle in water.

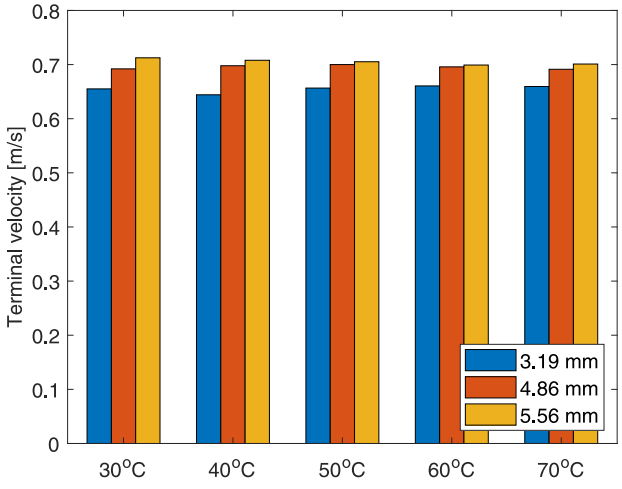

Fig. 4. Liquid gallium droplet's terminal velocity.

droplet image sequence ranging from 200 to 250 mm below the needle was selected to calculate the average droplet terminal velocity (u_T) and drag coefficient (C_D). In our experiments, we did not observe any significant difference in u_T by varying the temperature of liquid gallium and water as depicted in Figure 4 (further discussion in Sect. 3.4). However, it is obvious that the u_T is dependent on the droplet size.

3.3 Drag coefficient

Calculating the C_D was necessary to characterise the motion and the kinematics of the droplets. Firstly, a theoretical correlation to obtain C_D as a function of Reynolds number (Re) and fluid properties was developed. Then, experimental values obtained by image processing were used to calculate the C_D and the effect of deformation is subsequently investigated. A simple correlation based on net gravitational force (gravitational buoyancy) and drag force balance for a sphere at terminal

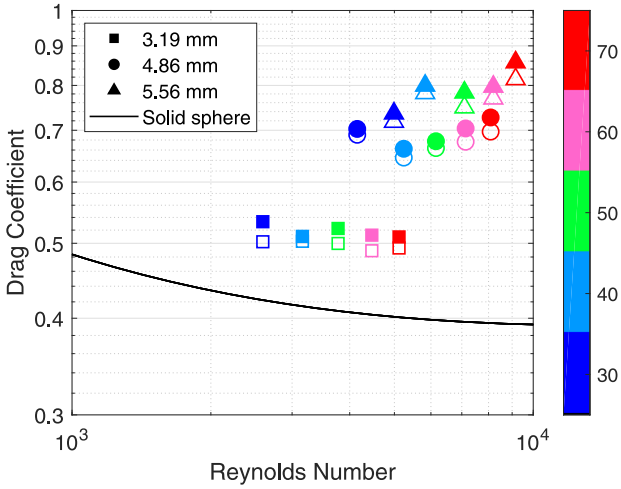

Fig. 5. The relationship between drag coefficient and Reynolds number (open symbols are experimental values and filled symbols are theoretical values).

condition are given by equation (1).

$$\pi(\rho_d - \rho_c)g\frac{d_{\text{eq}}^3}{6} = \frac{1}{8}C_D\pi d_{\text{eq}}^2\rho_c u_T^2. \quad (1)$$

Note that d_{eq} is used in this equation to remove the effect of deformation. Equation (1) can be rearranged to calculate C_D based on $C_D = f(Re)$ as follows:

$$C_D = \frac{4}{3}\frac{(\rho_d - \rho_c)\rho_c g d_{\text{eq}}^3}{\mu_c^2}/Re^2, \quad (2)$$

where $Re = \frac{\rho_c u_T d}{\mu_c}$ is the particle Re, μ_c and ρ_c are the continuous phase fluid viscosity and density, respectively, and d is the diameter of the droplet.

Next, C_D was derived from the experiment. In order to obtain the exact value of C_D, the droplet deformation was considered. Instead of d_{eq}, the droplet's actual frontal diameter obtained directly from the images through image processing was used. Figure 5 compares the C_D calculated from equation (2) with those from experiment along with the classical curve of C_D of a solid sphere. An acceptable agreement between theory and experiment was validated by the minimal discrepancy between theoretical and experimental values. The differences in those values may be due to the effect of deformation that has been ignored in the derivation of equation (2). Moreover, it is noted that as the Re increases, the experimental C_D values deviate from those calculated for an equivalent solid sphere and the difference is more pronounced for larger droplets.

3.4 Shape and deformation of droplet

The C_D of a falling droplet is known to be dependent upon the droplet shape. The shape of droplets experiencing free fall in an infinite medium under the influence of gravity are generally classified in three categories as shown in Figure 6. These categories are defined by the ratio of its largest horizontal dimension (equator), d_h, to its largest vertical

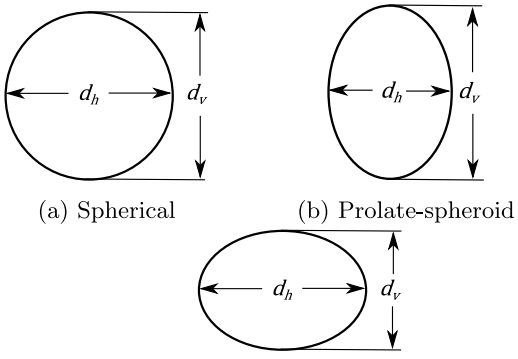

(a) Spherical (b) Prolate-spheroid

(c) Oblate-spheroid

Fig. 6. Schematic diagrams of typical droplet shape.

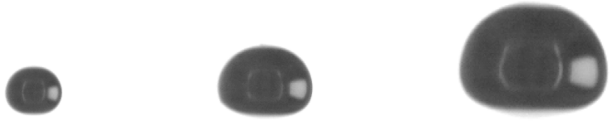

(a) 3.19 mm (b) 4.86 mm (c) 5.56 mm

Fig. 7. Shape of liquid gallium droplets at terminal condition.

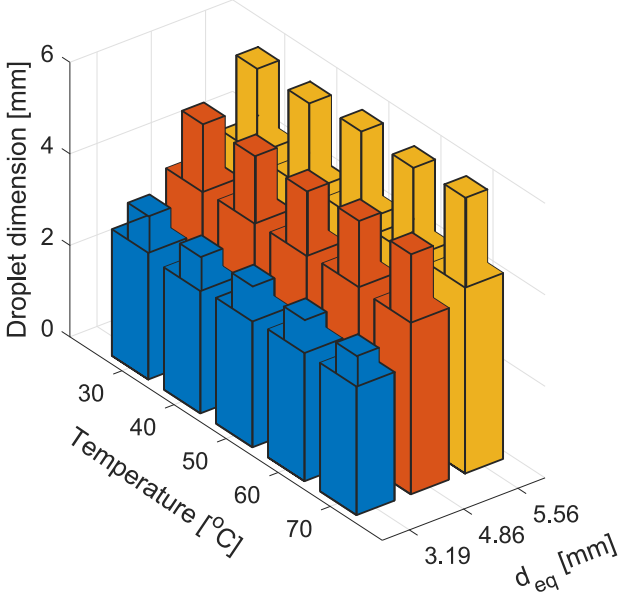

Fig. 8. Comparison of horizontal (thin bar) and vertical (wide bar) dimensions of liquid gallium droplet at different temperatures.

dimension (polar), d_v, known as aspect ratio, $E = \frac{d_h}{d_v}$. Droplets are classified as spherical if the aspect ratio lies within 10% of unity. For an aspect ratio other than that, droplet is described deformed and can be classified as an ellipsoid, which has two subcategories, namely oblate spheroid and prolate spheroid.

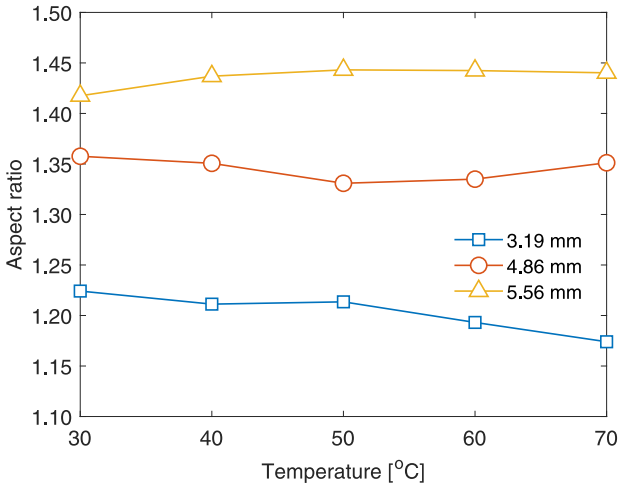

Fig. 9. Comparison of aspect ratio of liquid gallium droplet at different temperatures.

Figure 7 shows representative photographs of different sizes of liquid gallium droplets used in our experiment as they fall through water and Figure 8 illustrates the dimensions of those droplets obtained from image processing of the images for five sequences for each diameter. The gallium droplets are deformed even at the smallest diameter and the value of aspect ratio is always above 1.1 (see Fig. 9), thus we can classify all of the droplets as oblate spheroid. The deformation of the droplets from spherical shape can also be confirmed visually by looking the images in Figure 7. Due to aerodynamic and hydrostatic pressure, the droplet aspect ratio continues to increase with droplet diameter [15]. With the Re in the current investigation ranging from 10^3 to 10^4, this observation might extend the conclusion made by Taylor and Acrivos [16] to a wider range of Re – that a droplet is likely to be deformed into an oblate spheroid instead of a prolate spheroid for all cases at low Re. It is also noted that the temperature does not have a significant effect on the steady state shape of a liquid gallium droplet.

Deformation occurs because of the interplay between pressure distribution and surface tension. The pressure distribution produces local fluid-dynamic stresses, which are controlled by the viscosity ratio, λ (which controls the circulation inside droplet) and Re (which controls the importance of viscosity). Surface tension is affected by the Weber number (We), the ratio of continuous fluid stresses, which causes deformation to the surface tension stresses, which oppose deformation. These independent non-dimensional parameters can be calculated using the following equations:

$$\lambda = \frac{\mu_d}{\mu_c}, \tag{3}$$

$$We = \frac{\rho_c u^2 d}{\sigma_{c-d}}, \tag{4}$$

where μ_d is the dispersed fluid viscosity and σ_{c-d} is the interfacial surface tension between the dispersed and

Table 2. Physical parameters of the continuous and dispersed fluid.

$T(^{\circ}C)$	ρ_c	μ_c	ρ_d	μ_d	σ_{c-d}
30	995.7	0.798	6084	139.0	698.4
40	992.2	0.653	6077	137.7	698.1
50	988.0	0.547	6071	136.5	697.9
60	983.2	0.466	6064	135.2	697.5
70	977.8	0.404	6058	134.0	697.2

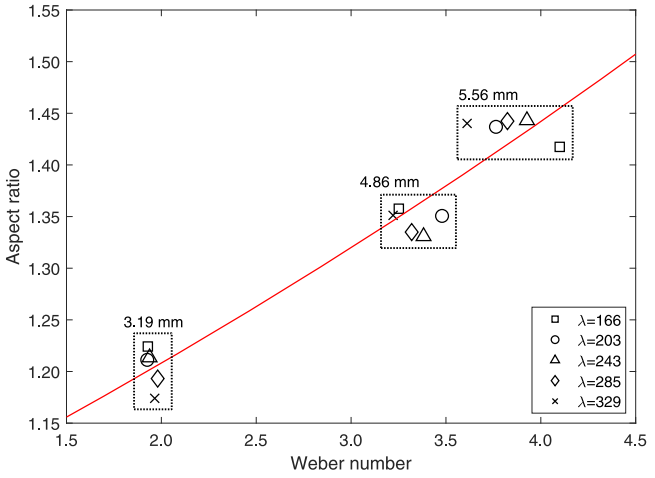

Fig. 10. The relationship between aspect ratio and Weber number for different viscosity ratio.

continuous fluid. This parameter could possibly be approximated by utilizing equation (5) [17]. Table 2 summarises the physical properties of liquid gallium and water at different temperatures that are relevant to the experiment.

$$\sigma_{c-d} = \sigma_d + \sigma_c - 2\sqrt{\sigma_c \sigma_d}. \quad (5)$$

Figure 10 shows the relationship between the aspect ratio and *We* for different λ. In our experiment, viscosity variation is caused by varying the temperature of the liquid gallium and water as shown in Table 2, producing a range of λ from 166 to 329. Internal circulation inside the droplet caused by the λ, which produces high pressure at the leading and trailing edge of the droplet, tends to cause prolate shapes. On the other hand, fluid surrounding the droplet also produces a high-pressure zone at the trailing and leading edges of the droplet and a low-pressure zone near the equator [18]. This opposes the effect of internal circulation and tends to cause oblate droplet shapes [19]. In our experiments, the viscosity of the dispersed fluid (liquid gallium) is relatively large compared to the continuous fluid (water), giving a high λ. This condition restricts the internal circulation, hence the droplets are deformed in an oblate. As expected, droplet deformation is very much less affected by the λ but is rather dependent on droplet size and *We* [18]. The correlation is found to

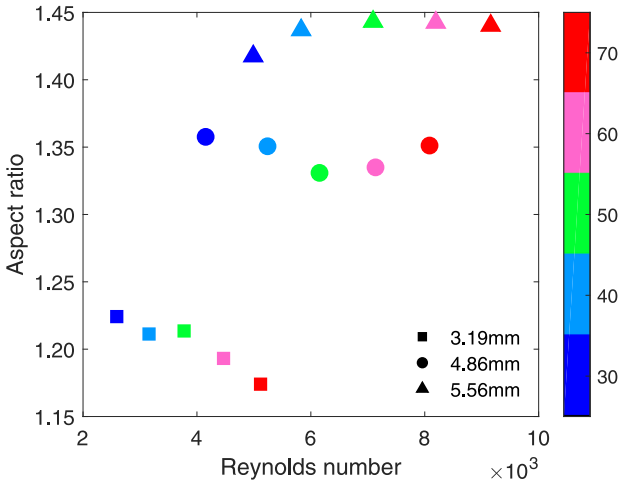

Fig. 11. The relationship between the aspect ratio and Reynolds number for different sizes of liquid gallium droplet.

follow a quadratic trend line:

$$E = 1.0122e^{0.0885We}. \quad (6)$$

For droplets with small values of *We*, the values of the aspect ratio are nearly 1.1 (nearly spherical) and tend to increase as the *We* increases. This trend indicates that at low *We*, the surface tension can counterbalance the continuous fluid stresses. However, as the *We* increases, the continuous fluid stresses become significant up to a point where the surface tension can no longer resist the deformation from occurring. This may also explain why no significant change in the u_T is observed. The restricted internal circulation increases the velocity gradient at the liquid–liquid interface, producing higher shear stresses at the interface. The effect of lower buoyancy force due to lower water viscosity caused by increasing temperature may be cancelled by the larger viscous dissipation between the phases. The overall effect is that the u_T is unaffected by the temperature range used for this experiment.

In order to further quantify the effect of pressure distribution on droplet deformation, the relationship between the aspect ratio and *Re* for different droplet sizes are plotted in Figure 11. While the data exhibit some scattering, the aspect ratio remains almost constant as a function of *Re* and depends more on droplet diameter. This phenomenon is most pronounced for $4000 < Re < 8000$, where *Re* for small and large diameter droplets overlap. At constant d_{eq} and u_T, only two parameters in *Re* were varied by temperature: ρ_c and μ_c. Based on this, we can say that viscous force has a negligible effect on droplet deformation. Hence, it is reasonable to conclude that droplet shape and deformation are influenced mainly by interfacial surface tension and inertial force and is less affected by viscous force and pressure distribution. This conclusion is similar to the Hadamard–Rybczynski solution, which states that pressure distribution due to viscous force does not produce deformation for Stokes flow over a droplet and that a droplet of liquid is only affected by viscosity minimally [10,16].

4 Conclusion

An experimental study has been conducted on the effect of shape and deformation on u_T and C_D of free-falling liquid gallium droplet in water at terminal condition. Liquid gallium and water were held at temperatures in the range 30–70 °C, selected in order to produce a significant variation in physical properties (density, viscosity and surface tension). A simple theoretical C_D correlation was proposed and then compared with the experimental data. The d_{eq} was used in the correlation to calculate the C_D. Considering the error caused by the assumption that the droplet remains spherical, the correlation agrees well with empirical data of C_D for droplets with a Re in the range $10^3 < Re < 10^4$. Consequently, the effect of three independent non-dimensional parameters, namely, viscosity ratio, Weber number and Reynolds number on the dynamic droplet shape, which has a direct influence on C_D, were examined. It was found that for $We < 4.5$, the shape of droplets tend to deform into an oblate spheroid. The oblateness was seen to increase in extent with the We. The droplet shape and deformation are strongly dependent on the interfacial surface tension and inertial force, in contrast to pressure distribution and λ, which have a negligible effect.

Authors contribution statement

All the authors were involved in the preparation of the manuscript. All the authors have read and approved the final manuscript.

References

1. G. Edara, Y.V. Murthy, K.V. Sharma, S. Pullela, Case Stud. Thermal Eng. **10**, 121 (2017)
2. A. Ono, T. Kawai, J. Photopolym. Sci. Technol. **23**, 363 (2010)
3. R. Seemann, M. Brinkmann, T. Pfohl, S. Herminghaus, Rep. Prog. Phys. **75**, 016601 (2012)
4. J. Oh, P. Birbarah, T. Foulkes, S.L. Yin, M. Rentauskas, J. Neely, R.C. Pilawa-Podgurski, N. Miljkovic, Appl. Phys. Lett. **110**, 1 (2017)
5. H. Ge, J. Liu, J. Heat Transf. **135**, 054503 (2013)
6. Q. Wang, Y. Yu, J. Yang, J. Liu, Adv. Mater. **27**, 7109 (2015)
7. X. Li, M. Li, L. Zong, X. Wu, J. You, P. Du, C. Li, Adv. Funct. Mater. **28**, 1 (2018)
8. L. Hines, K. Petersen, G.Z. Lum, M. Sitti, Adv. Mater. **29** (2017), doi: 10.1002/adma.201603483
9. M. Yunusa, G.J. Amador, D.M. Drotlef, M. Sitti, Nano Lett. **18**, 2498 (2018)
10. M. Clift, R. Grace, J.R. Weber, J. Fluid Mech. **94**, 795 (1978)
11. E. Loth, Int. J. Multiphase Flow **34**, 523 (2008)
12. M. Wegener, N. Paul, M. Kraume, Int. J. Heat Mass Transf. **71**, 475 (2014)
13. P. Uhlherr, R. Chhabra, Can. J. Chem. Eng. **73**, 918 (1995)
14. P.P. Brown, D.F. Lawler, J. Environ. Eng. **129**, 222 (2003)
15. C. Béguin, S. Étienne, M.J. Pettigrew, Eur. J. Mech. B **65**, 339 (2017)
16. T.D. Taylor, A. Acrivos, J. Fluid Mech. **18**, 466 (1964)
17. Y.M. Jung, H.C. Oh, I.S. Kang, J. Colloid Interface Sci. **322**, 617 (2008)
18. B.T. Helenbrook, C.F. Edwards, Int. J. Multiphase Flow **28**, 1631 (2002)
19. B.T. Helenbrook, in *ILASS Americas 14th Annual Conference on Liquid Atomization and Spray Systems*, Dearborn, MI, May, 2001.

Cite this article as: M. Sofwan Mohamad, C.M. Mackenzie Dover, K. Sefiane, Experimental investigation of drag coefficient of free-falling deformable liquid gallium droplet, Eur. Phys. J. Appl. Phys. **84**, 10903 (2018)